Scientific Journal of Silesian University of Technology. Series Transport
Zeszyty Naukowe Politechniki Śląskiej. Seria Transport

Volume 104 **2019**

p-ISSN: 0209-3324

e-ISSN: 2450-1549

DOI: https://doi.org/10.20858/sjsutst.2019.104.14

Journal homepage: http://sjsutst.polsl.pl

Article citation information:
Štalmach, O., Dekýš, V., Novák, P., Sapieta, M. Processing of results from a thermal FEM analysis using the lock-in method and comparison with experiment. *Scientific Journal of Silesian University of Technology. Series Transport*. 2019, **104**, 159-168. ISSN: 0209-3324. DOI: https://doi.org/10.20858/sjsutst.2019.104.14.

Ondrej ŠTALMACH[1], Vladimír DEKÝŠ[2], Pavol NOVÁK[3], Milan SAPIETA[4]

PROCESSING OF RESULTS FROM A THERMAL FEM ANALYSIS USING THE LOCK-IN METHOD AND COMPARISON WITH EXPERIMENT

Summary. This article dealt with the comparison of results obtained from an experiment and from the numerical thermal FEM analysis. Sample with defects were printed on a 3D printer. A thermal wave from the halogen lamp to excite the front surface of the sample was used in the next step and the response was measured by a thermal camera. After processing the data in the software DisplayIMG, a phase image was created representing the 2D image of the material at a certain depth under the surface of the model. Lock-in method was applied to the results from the numerical thermal FEM analysis and the phase image was created. The programs code were created in MATLAB for a 4 points, multiple points and differential lock-in method which were compared with the results from the experiment.

Keywords: lock-in method, thermal FEM analysis, thermography, thermal excitation

[1] Faculty of Mechanical Engineering, University of Zilina, Univerzitná 1, 010 26 Žilina, Slovakia. Email: ondrej.stalmach@fstroj.uniza.sk
[2] Faculty of Mechanical Engineering, University of Zilina, Univerzitná 1, 010 26 Žilina, Slovakia. Email: ondrej.stalmach@fstroj.uniza.sk
[3] Faculty of Mechanical Engineering, University of Zilina, Univerzitná 1, 010 26 Žilina, Slovakia. Email: ondrej.stalmach@fstroj.uniza.sk
[4] Faculty of Mechanical Engineering, University of Zilina, Univerzitná 1, 010 26 Žilina, Slovakia. Email: ondrej.stalmach@fstroj.uniza.sk

1. INTRODUCTION

With the greater availability and rapid decline in the prices of thermal cameras in the last years, thermography has developed from being a rarely used technique to an increasingly popular investigation method. There are a number of techniques for evaluating the time dependence of temperature distribution.

Experimental methods often utilise the detection of a test object's response to excitation. An infrared camera (IRC) can also be used as a detector for these measurements. Using a camera in the 3-5 um (MWIR) wavelength range with an InSb detector, it is possible to detect events with microsecond integration times. This can be used to detect the occurrence of fast events, for example, Lüders bands [1-3], when synchronizing the camera with exciting harmonic loading events, which is useful in thermoelastic analysis (TSA) [4,5], in determining the dissipative energy estimation in fatigue tests [6,7,8], determining crack size [9], in the analysis of vibration and determination of resonance frequencies and modal shapes [10,11].

In thermoelastic analysis, the temperature change during the adiabatic loading cycle (when the minimum frequency for steel is 2 Hz, for Al alloys 20 Hz) is usually very low at the ICR noise level. Increase in signal-to-noise ratio is achieved by lock-in technology [12] processing the camera output. This increases the sensitivity by at least 1 order, which is sufficient for determining temperature change. In the elastic region, based on the linear relationship between the temperature change and the trace of stress tensor, it is possible to determine the distribution of the sum of the principal stresses on the test object [13].

In cyclic loading, if there is only microplastic deformation below the fatigue limit, the radiation level corresponding to the dissipated energy of the detected IRC is approximately constant and is a linear function of the mean and load amplitudes. When the load is higher than the limit, this energy increases, which is detectable by the camera. The breakpoint determines the fatigue limit and the energy corresponding to the linear dependencies (before and after the breakpoint) and the Wöhler curve can also be determined [14]. Such a test is an accelerated fatigue test with loading in blocks of increasing mean and amplitude, with the radiated energy rate determined in each block. This also makes it possible to analyse the formation and propagation of the plastic region in the crack root [15,16].

The application of the MWIR IRC is significant in non-destructive testing (NDT) when the excitation is realised, for example, cyclic loading (fatigue testing machine), sonotrode (ultrasound) and temperature waves (halogen reflector). Response is detected by IRC using lock-in. The output is interpreted as the amplitude and phase of the Fourier series at lock-in frequency corresponding to the excitation frequency [12]. Through the phase change, the defects in the object are detectable. The excitation frequency determines the depth of defect below the surface [17].

A separate issue is a multi-parametric approach, where temperature dependence measurement is also used to assess the reliability of the technology [18-25].

While the steady-state thermography is often called "passive thermography", the techniques evaluating dynamic temperature are called "active thermography", since the sample temperature is actively influenced by certain means. The most prominent examples of this class of non-steady-state or dynamic thermography are the pulse and lock-in thermography.

2. LOCK-IN METHOD

The lock-in principle is the technique of choice, if signals have to be extracted from statistical noise. Prerequisite to using this technique is that the primary signal, can be periodically pulsed or anyhow else amplitude-modulated with a certain frequency called "lock-in frequency" $f_{lock-in}$ [12]. The lock-in method uses the non-destructive testing by infrared thermography to detect the hidden defects in the sample. In this case, it is necessary to synchronise the modulated signal of the heat source with measured data. Moreover, the lock-in method is used, for example, in mechanics, in determining deformation fields, or for determining the fatigue limit.

Lock-in method can be described as a multiplication of detected signal F by a weighting factor K. This process is usually called lock-in correlation procedure. Output signal S for synchronous correlation is obtained by linear averaging over n lock-in periods (L is phase position, N is number of frames in one period):

$$S^L = \frac{1}{nN}\sum_{i=1}^{n}\sum_{j=1}^{N} K_j^L F \tag{1}$$

The correlation function optimum to achieve the best signal to noise ratio is the harmonic function. When we use sine wave with amplitude A and its phase φ we get:

$$F(t) = Asin(2\pi f_{lock-in}t + \varphi) = Asin(2\pi f_{lock-in}t)\cos\varphi + Acos(2\pi f_{lock-in}t)\sin\varphi \tag{2}$$

And weight factors are:

$$K_j^{0^\circ} = 2\sin\left(\frac{2\pi(j-1)}{n}\right) \tag{3}$$

$$K_j^{90^\circ} = 2\cos\left(\frac{2\pi(j-1)}{n}\right) \tag{4}$$

Using the addition theorem of equation (2) and equations (3) and (4) the results of correlation are [18]:

$$S^{0^\circ} = A\cos\varphi \tag{5}$$

$$S^{90^\circ} = A\sin\varphi \tag{6}$$

Then, the amplitude a the phase are [9,10]:

$$A = \sqrt{(S^{0^\circ})^2 + (S^{90^\circ})^2} \tag{7}$$

$$\varphi = \tan^{-1}\left(\frac{S^{90^\circ}}{S^{0^\circ}}\right) \tag{8}$$

3. EXPERIMENT

One of the purposes of this paper is to design a 3D model with the defects (Fig. 1) that is printed on a 3D printer (Mark Two). The defects are designed like blind holes 10x10 mm with the square cross section with the different depth under the surface the model. The samples are printed from the material "Onyx" which is defined by the producer as nylon mixed with chopped carbon fibre. The macroscopic properties of the composite materials are converted from the material properties of the components by homogenisation techniques, for example, in this case, are taken the parameters of the basic material because the manufacturer did not provide sufficient documentation. The thermal properties of the Onyx are:

- density $\rho = 1.18\ g/cm^3$

- isotropic thermal conductivity $\kappa = 0.23$ *W/(m.K)*
- specific heat $c_p = 1510$ *J/(kg.K)*

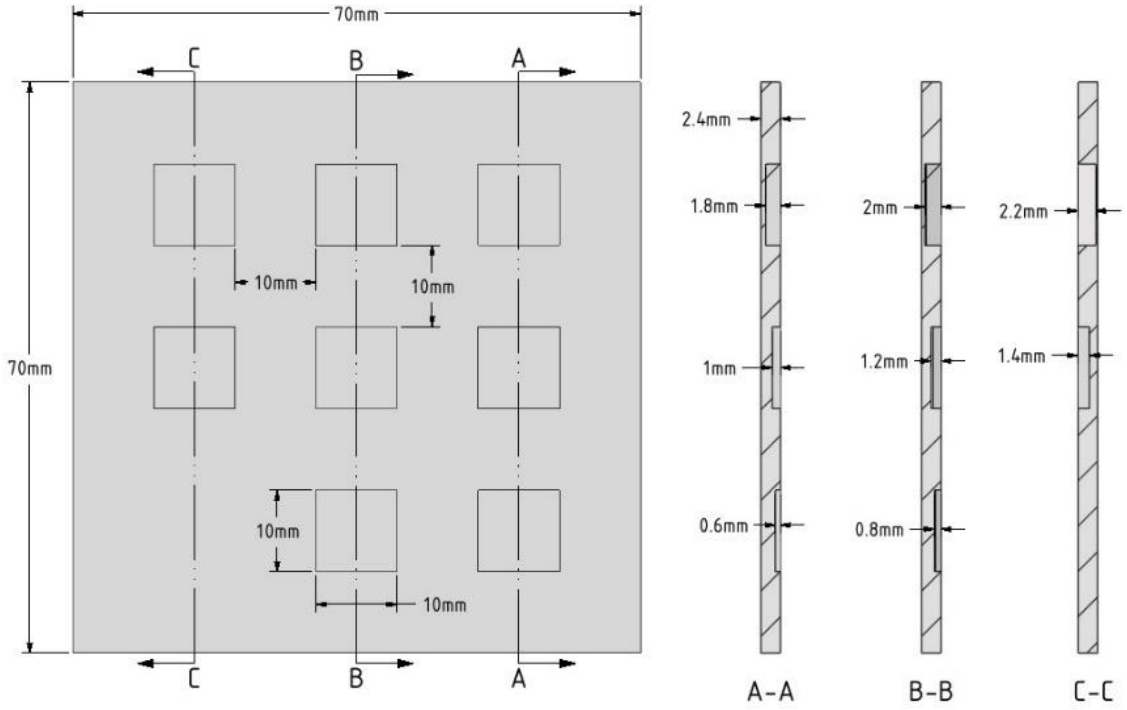

Fig. 1. 3D model with the defects

Experiment is done using the optical excited lock in thermography and the goal is for detection of defects in the specific depth under the surface. The basic idea of lock-in thermography (Fig. 2) is the visualisation of thermal wave propagation. The phase angle of such waves provides information about thermal structures and inhomogeneities. The thermal waves are generated by intensity-modulated halogen lamps which heat up the surface. The signal is captured by a high-resolution infrared camera. The evaluation method "R/L-Algorithm" allows for the determination of thicknesses and thermal reflection coefficients. A sinusoidal thermal source is used to excite the surface of a sample. The thermal excitation source consisted of one halogen lamp of 2.5 kW, driven by a power amplifier and a function generator.

In addition to optical excitation, which is considered optimal for composites, other types are also used, such as ultrasonic excitation of metallic materials.

For detection of thermal waves, a thermal camera FLIR SC7500 with cooled detector was used. This IR camera has a temperature resolution of 20 mK and 320 x 256 pixel resolution. The camera is attached to the thermal source, which is used to generate harmonic waves passing the sample with adequate frequency. The thermal camera frame rate is set to 100 frames per second.

In the DisplayIMG software, measured data from the thermal camera are processed using the lock-in method and the result is the phase image. Lock in frequency is used to determine reaction at certain depth μ under the surface of the measured sample:

$$\mu = \sqrt{\frac{2\kappa}{2\pi\rho c_p f_{Lock-in}}} \tag{9}$$

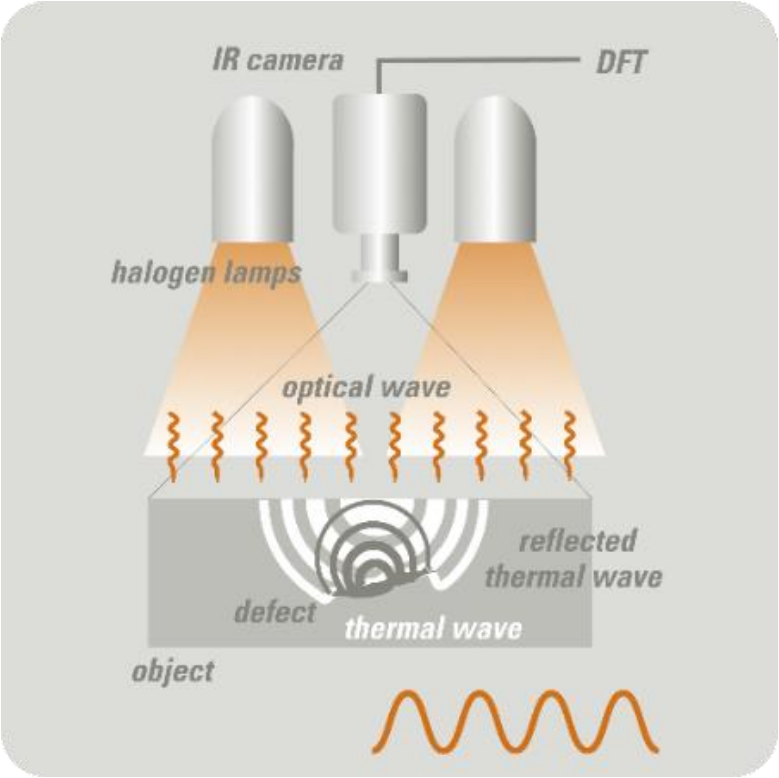

Fig. 2. Principle of optically excited Lock-in thermography

Lock-in frequency is same as the frequency of the stimulated thermal wave. In this experiment,the lock-in frequency was set to 0.1719 Hz which represents the reaction from the depth around 0.5 mm under the surface. Configuration of devices which were used in the experiment is shown in Fig. 3a). The phase image which was getted from the DisplayING was imported to Matlab and a 176 x 176 image is cropped from the 320 x 256 image showing only samples without the other background (Fig. 3b).

4. NUMERICAL FEM SIMULATIONS

Sample with the defects (Fig. 1) is stimulated by the heat flux with the cosines amplitude in the program Ansys workbench. This thermal simulation represented an experiment in which the model is stimulated by the heat flux using the halogen lamp. On the front surface of the model is applied the heat flux *M*, which represent the thermal wave used in the experiment. Maximum of the heat flux amplitude is 12.8 W/m^2 which is computed from the data of power of the halogen lamp used in the experiment. Cosine wave of the heat flux is applied using the data in Tab. 1. On the other surfaces of the sample is applied the convection which represents a natural heat transfer between the object and the ambient air and its value is 20 $W/m^2.K$.

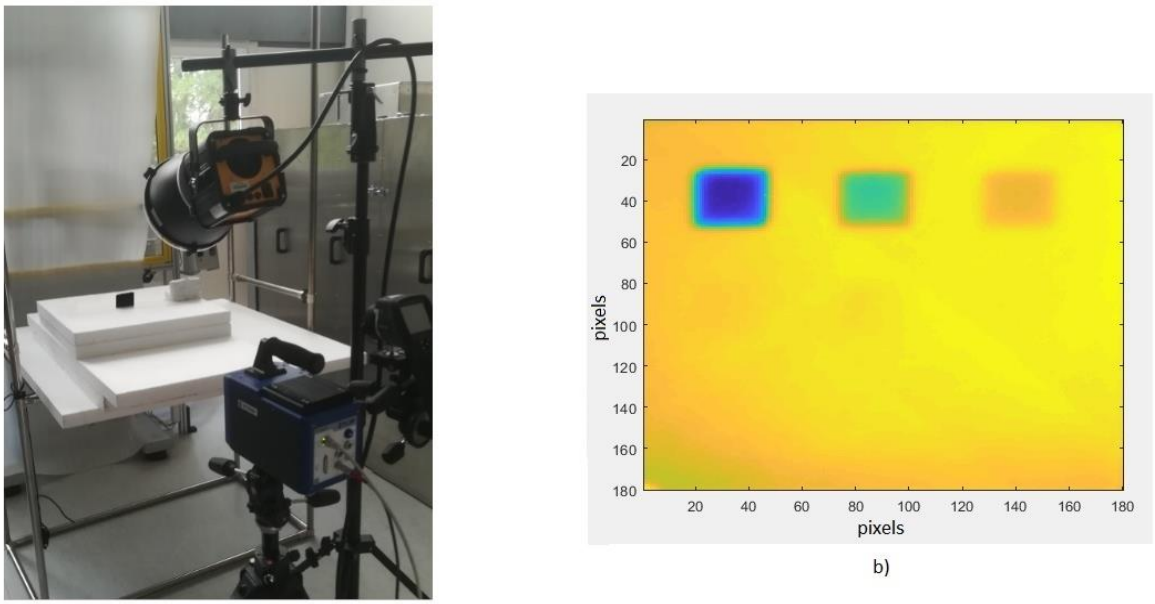

Fig. 3. Configuration of the devices (a), and phase image from the experiment (b)

Tab. 1

Values of the heat flux M across the time t

	1.	2.	3.	4.	5.	6.	7.	8.	9.	10.
t [s]	0	0.646	1.292	1.939	2.585	3.231	3.878	4.524	5.171	5.817
M [W/m^2]	0	1.497	5.288	9.6	12.414	12.414	9.6	5.288	1.497	0

On the front surface of the numerical model of the sample was created the mapped mesh 176 x 176 nodes, which represent the 176 x 176 pixels of the thermal camera covering the surface of the sample. The final numerical mesh contained 635 072 nodes, 133 125 elements and was made up of the hexahedral linear elements. The boundary conditions are shown in Fig. 4.

After the simulations, the nodes on the front surface (176 x 176) and its values of the temperature were exported to the text file. It is done for the every time step from the Tab. 1. From these text files were created 2D matrices, which represent the distribution of the temperature on the front surface of the sample. It is similar to the image created by the thermal camera. After processing these images using the lock-in method, the phase images were created. Three methods of lock-in were used:

- four points lock-in method which uses only the four images at the position 2, 4, 6, 8 (Fig. 5a)
- multiple points lock-in method which uses all the images (Fig. 5b)
- differential lock-in method which on the beginning subtract the first image from the others than is calculated from this differential images (Fig. 5c)

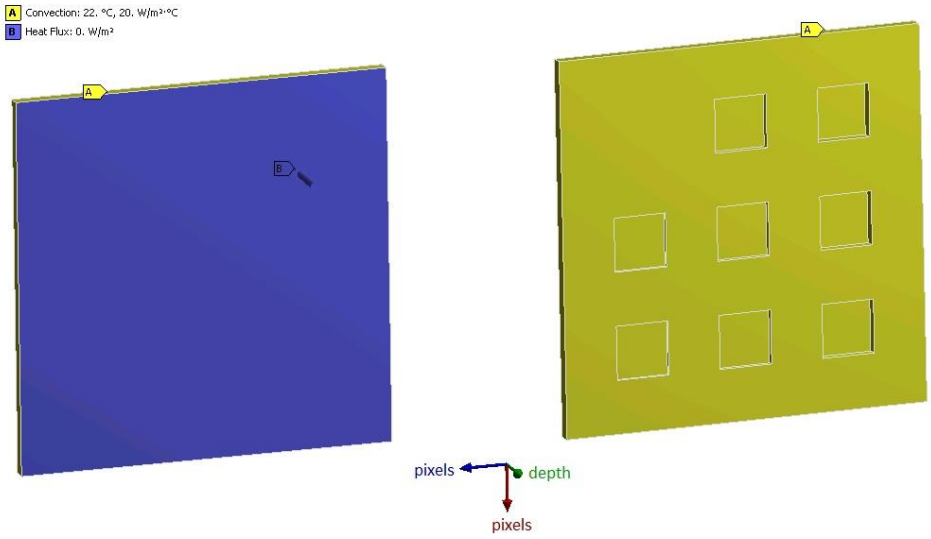

Fig. 4. Front surface (blue) and the others

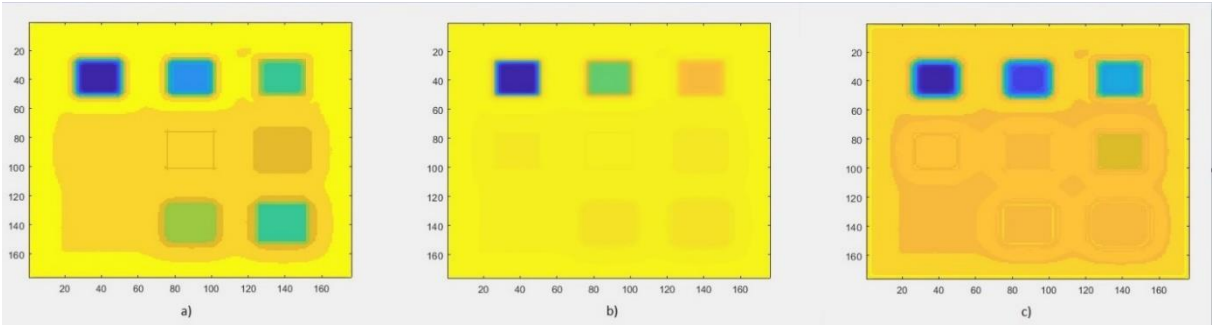

Fig. 5. Four points lock-in (a), multiple points lock-in (b), and differential lock-in (c)

The phase images look identical like the phase image from the experiment. To determine the deviations of these three results from the measured result of the experiment, it is necessary to select a line (profile) from all of these phase images that are on the y-axis at the position 40 (red arrow). These lines are after that normalise because of comparison on the same scale. The results are shown in Fig. 6.

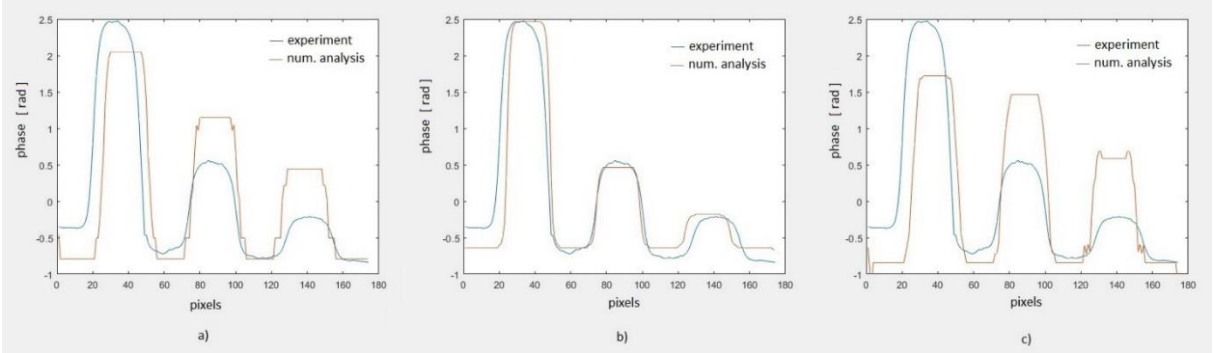

Fig. 6. Four points lock-in vs. experiment (a), multiple points lock-in vs. experiment (b), and differential lock-in vs. experiment (c)

In the table are shown the percentage differences between the three peaks of the line from the experiment and from the numerical simulation.

Tab. 2

Differences between the lines

	Experiment (blue line)	Numerical simulation (red line)	Absolute differences
Peak a) (Left)	2.46	2.05	0.41
Peak a) (Middle)	0.55	1.15	0.6
Peak a) (Right)	- 0.22	0.45	0.67
Peak b) (Left)	2.46	2.46	0
Peak b) (Middle)	0.55	0.46	0.09
Peak b) (Right)	- 0.22	- 0.17	0.05
Peak c) (Left)	2.46	1.72	0.74
Peak c) (Middle)	0.55	1.47	0.92
Peak c) (Right)	- 0.22	0.59	0.81

From these results, it is obvious that the multiple points lock-in method is closest to the experiment. This is because the software DisplayIMG also uses this method to process data from the infrared camera. This method is the closest to reality because when the lock-in frequency 0.1719 Hz is used to represent the reaction from the depth around 0.5 mm under the surface, only the first two defects were seen.

5. CONCLUSION

In this article, the sample with defects was printed on a 3D printer and was used for the optical lock-in thermography. Also using this model, the numerical FEM simulation representing this optical lock-in thermography was created. A sinusoidal thermal source (halogen lamp) was used to excite the surface of the sample and a thermal camera FLIR SC7500 was used for detection. The phase image was getted from the DisplayING. Phase image representing the 2D image of the material at a depth 0.5 mm (because lock-in frequency is 0.1719 Hz) under the surface of the model. After processing, the data from the experiment and numerical simulation was created. In MATLAB, was created programs for 4 points, multiple points and differential lock-in method, which were used to process data from the numerical simulation. These methods were compared to the experiment. The multiple points lock-in method is the closest to the experiment and reality. Therefore, this method can be used in future research.

Acknowledgements

This paper was supported by KEGA 017ŽU-4/2017 and by the Slovak Research and Development Agency under contract No. APVV–0736–12.

References

1. Louche Hervé, André Chrysochoos. 2001. „Thermal and dissipative effects accompanying Lüders band propagation". *Materials Science and Engineering* 307(1-2): 15-22. ISSN 0921-5093. DOI: https://doi.org/10.1016/S0921-5093(00)01975-4.
2. Srinivasan Nagarajan, N. Raghu, Balasubramanian Venkatraman. 2012. "Study on lüders deformation in welded mild steel using infrared thermography and digital image correlation". *Advanced Materials Research* 585: 82-86. ISSN 1662-8985. DOI: https://doi.org/10.4028/www.scientific.net/AMR.585.82.
3. Brlić Tin, Stoja Rešković, Ivan Jandrlić, Filip Skender. 2018. „Influence of strain rate on stress changes during Lüders bands formationand propagation". *IOP Conference Series: Materials Science and Engineering* 461(1): 012007. ISSN: 1757-899X. DOI: doi:10.1088/1757-899X/461/1/012007.
4. Chandraprakash Chindam, Chitti Venkata Krishnamurthy, Krishnan Balasubramaniam. 2019. „Thermomechanical phenomenon: a non-destructive evaluation perspective". *Transactions of the Indian Institute of Metals*: 1-11. ISSN 0975-1645. DOI: https://doi.org/10.1007/s12666-019-01656-6.
5. Patterson Eann A., Robert E. Rowlands. 2008. „Determining individual stresses thermoelastically". *The Journal of Strain Analysis for Engineering Design* 43(6): 519-527. ISSN 0309-3247. DOI: https://doi.org/10.1243/03093247JSA358.
6. Fargione Giovanna, Alberto Geraci, Guido La Rosa, Antonino Risitano. 2002. „Rapied determination of the fatigue curve by the thermographic method". *International Journal of Fatigue* 24(1): 11-19. ISSN 0142-1123. DOI: 10.1016/S0142-1123(01)00107-4.
7. De Finis Rosa, Davide Palumbo, Francesco Ancona, Umberto Galietti. 2015. „Fatigue limit evaluation of various martensitic stainless steels with new robust thermographic data analysis". *International Journal of Fatigue* 74: 88-96. ISSN 0142-1123. DOI: https://doi.org/10.1016/j.ijfatigue.2014.12.010.
8. Sága, Milan, Peter Kopas, Milan Uhríčik. 2012. „Modeling and experimental analysis of the aluminium alloy fatigue damage in the case of bending - torsion loading". *Procedia Engineering* 48: 599-606. ISSN 1877-7058. DOI: https://doi.org/10.1016/j.proeng.2012.09.559.
9. Ju Shen-Haw, Robert E. Rowlands. 2007. "Thermoelastic determination of crack-tip coordinates in composites". *International Journal of Solid and Structures* 44 (14-15): 4845-4859. ISSN 0020-7683. DOI: https://doi.org/10.1016/j.ijsolstr.2006.12.003.
10. Montanini Roberto, Fabrizio Freni. 2013. „Correlation between vibrational mode shapes and viscoelastic heat generation in vibrothermography". *NDT & E International* 58: 43-48. ISSN 0963-8695. DOI: https://doi.org/10.1016/j.ndteint.2013.04.007.
11. Sága Milan, Róbert Bednár, Milan Vaško. 2011. „Contribution to modal and spectral interval finite element analysis". In: *Vibration Problems ICOVP 2011 Springer Proceedings in Physics* 139, edited by Jiří Náprstek, Jaromír Horáček, Miloslav Okrouhlík, Bohdana Marvalová, Ferdinand Verhulst, Jerzy T. Sawicki, 269-274. Springer, Dordrecht. ISBN 978-94-007-2069-5. DOI: https://doi.org/10.1007/978-94-007-2069-5_37.
12. Breitenstein Otwin, Warta Wilhelm, Langenkamp Martin. 2010. *Lock-in thermography*. Springer Series in Advanced Microelectronics. 2. Edition. ISBN 978-3-642-02416-0.
13. Dulieu-Barton Janice M. 1999. „Introduction to thermoelastic stress analysis". *Strain* 35(2): 35-40. ISSN 0039-2103. DOI: https://doi.org/10.1111/j.1475-1305.1999.tb01123.x.

14. Micone Nahuel, Wim De Waele. 2017. „On the application of infrared thermography and potential drop for the accelerated determination of an S-N Curve". *Experimental Mechanics* 57(1): 143-153. ISSN 0014-4851. DOI: https://doi.org/10.1007/s11340-016-0194-6.
15. Jones Rhys, Susane Pitt. 2006. „An experimental evaluation of crack face energy dissipation". *International Journal of Fatigue* 28(12): 1716-1724. ISSN 0142-1123. DOI: https://doi.org/10.1016/j.ijfatigue.2006.01.009.
16. Pottier Thomas, Franck Toussaint, Hervé Louche, Pierre Vacher. 2013. „Inelastic heat fraction estimation from two successive mechanical and thermal analyses and full-field measurements". *European Journal of Mechanics - A/Solids* 38: 1-11. ISSN: 0997-7538. DOI: https://doi.org/10.1016/j.euromechsol.2012.09.002.
17. Vavilov Vladimir. 2009. „Thermal / Infrared testing". In *Nondestructive testing*, edited by Klyuev Vitaly V, 11-452. Volume 5. Book 1. Russia: Spektr, ISBN 978-8-904270-01-8.
18. Kekez Michal, Leszek Radziszewski, Leszek, Alzbeta Sapietova. 2015. „Fuel type recognition by classifiers developed with computational intelligence methods using combustion pressure data and the crankshaft angle at which heat release reaches its maximum". *Procedia Engineering* 136: 353-358. ISSN 1877 7058. DOI: https://doi.org/10.1016/j.proeng.2016.01.222.
19. Žuľová Lucia, Robert Grega, Jozef Krajňák, Gabriel Fedorko, Vieroslav Molnár. 2017. "Optimization of noisiness of mechanical system by using a pneumatic tuner during a failure of piston machine". *Engineering Failure Analysis* 79: 845-851. ISSN 1350-6307.
20. Sapietova Alzbeta, Milan Saga, Ivan Kuric, Stefan Vaclav. 2018. „Application of optimization algorithms for robot systems designing". *International Journal of Advanced Robotic Systems* 15(1): 1729881417754152. ISSN 1729-8814. DOI: https://doi.org/10.1177/1729881417754152.
21. Bakowski Andrzej, Michal Kekez, Leszek Radziszewski, Alzbeta Sapietova. 2018. „Vibroacoustic real time fuel classification in diesel engine". *Archives of Acoustics* 43(3): 385-395. ISSN 0137-5075. DOI: 10.24425/123910.
22. Homišin J., R. Grega, P. Kaššay, G. Fedorko, V. Molnár. 2019. "Removal of systematic failure of belt conveyor drive by reducing vibrations". *Engineering Failure Analysis* 99: 192-202. ISSN 1350-6307.
23. Grega, R., J. Krajňák, L. Žuľová, G. Fedorko, V. Molnár. 2017. "Failure analysis of driveshaft of truck body caused by vibrations". *Engineering Failure Analysis* 79: 208-215. ISSN 1350-6307.
24. Maldague Xavier, P.V., Moore Patric O. 2001. *Nondestructive testing handbook: infrared and thermal testing*. 3. Edition. Amer Society for Nondestructive. ISBN: 1-57117-044-8.
25. Urbanský M., J. Homišin, P. Kaššay, M. Moravič. 2016. "Influence of piston compressor inner failure on mechanical system objective function". *Diagnostyka* 17(3): 47-52. ISSN 1641-6414.

Received 17.05.2019; accepted in revised form 17.08.2019